Cement and Concrete Research 40 (2010) 14–26

Contents lists available at ScienceDirect

Cement and Concrete Research

journal homepage: http://ees.elsevier.com/CEMCON/default.asp

Nanogranular packing of C–S–H at substochiometric conditions

Matthieu Vandamme [a,1], Franz-Josef Ulm [a,*], Philip Fonollosa [b]

[a] Massachusetts Institute of Technology, Cambridge MA
[b] Lafarge Research Center, L'Isle d'Abeau, France

ARTICLE INFO

Article history:
Received 12 February 2009
Accepted 21 September 2009

Keywords:
Nanoindentation (B)
C–S–H packing density (B)
Mix compositions (C)
Heat treatment (A)
Microstructure (B)

ABSTRACT

Herein, we present a comprehensive nanoindentation investigation of cement pastes prepared at substoichiometric water-to-cement (w/c) mass ratios between 0.15 and 0.4 with and without heat treatment. Based on a statistical indentation technique, we provide strong evidence of the existence of a statistically significant third hydrated mechanical phase in addition to the already known Low-Density (LD) and High-Density (HD) C–S–H phases. The nanomechanical properties of this third phase are found to follow similar packing density scaling relations as LD C–S–H and HD C–S–H, while being significantly greater. This third phase, whose nano-packing density is measured at 0.83 ± 0.01, is therefore termed Ultra-High-Density (UHD) phase. All three phases are present in concrete materials in different volume proportions: LD dominates cement-based materials prepared at high *w/c* mass ratios; HD and UHD control the microstructure of low *w/c* ratio materials. In addition, heat treatment favors the formation of HD and UHD. The insight thus gained into the link between composition, processing and microstructure makes it possible to monitor packing density distributions of the hydration products at the nanoscale.

1. Introduction

The increasing use of low water-to-cement ratios (w/c) in commercial cement-based material systems requires a reassessment of the link between composition, microstructure and mechanical performance of these materials. Groundbreaking contributions date back to the 1950s with the work of Powers and Brownyard [1], who by correlating macroscopic strength [2] and stiffness data [3] with physical data of a large range of materials prepared at different (w/c)-ratios early on recognized the critical role of the C–S–H porosity (or gel porosity), respectively the C–S–H packing ('one minus porosity') on the macroscopic mechanical behavior; in particular for cement pastes below a water-to-cement ratio of $w/c < 0.42$, for which the entire porosity of the material is situated within the C–S–H (no 'capillary water' in Powers' terminology), and for which the hydration degree α of the hardened material is smaller than one. Powers considered the C–S–H gel porosity (gel pore volume over total gel volume) to be material invariant and equal to $\varphi_0 = 0.28$ independent of mix proportions, hydration degree, C–S–H morphology, etc. The application of advanced microscopy, X-ray mapping and Neutron scattering techniques to cement-based materials later on revealed that the assumption of a constant gel porosity could not be but an oversimplification of the highly heterogeneous microstructure of cement-based materials, overlooking the particular organizational feature of cement hydration products in highly dense packed 'inner' products and loosely packed 'outer' products (see, for instance [4–14]). The quantitative translation of these morphological observations into a concise colloidal model of the gel microstructure is due to Jennings et al. [15–19] who recognized that outer and inner products are two structurally distinct but compositionally similar C–S–H phases; that is, amorphous nanoparticles of some 5 nm characteristic size pack into two characteristic forms, a Low-Density (LD) C–S–H phase and a High-Density (HD) C–S–H phase, that can be associated with outer and inner products. The existence and mechanical importance of these phases have been confirmed by nanoindentation [20–22]: LD C–S–H and HD C–S–H were found to be uniquely characterized by a set of material properties that do not depend on mix proportions, type of cement etc. Instead, they are intrinsic material invariant properties. The link between these mechanical C–S–H phase properties and C–S–H packing density has been established, showing that the C–S–H phases exhibit a unique nanogranular morphology [18,23–25], with packing densities that come remarkably close to *limit* packing densities of spheres; namely the random close-packed limit (RCP, [26]) or maximally random jammed state (MRJ, [27]) of $\eta \approx 0.64$ for the LD C–S–H phase, and the ordered face-centered cubic (fcc) or hexagonal close-packed (hcp) packing of $\eta = \pi / \sqrt{18} \approx 0.74$ [28] for the HD C–S–H phase. Far from being constant, the gel porosity of the C–S–H phase is recognized to depend on the volume proportions of LD C–S–H (f_{LD}) and HD C–S–H (f_{HD}); $\varphi_0 = 1 - (0.64 \times f_{LD} + 0.74 \times f_{HD})$. All these findings have been established for cement pastes at or above the stoichiometric limit of $w/c = 0.42$, and little is known on how the C–S–H packing densities, gel

* Corresponding author. Tel.: +1 617 253 3544.
E-mail address: ulm@mit.edu (F.-J. Ulm).
[1] Now at Ecole des Ponts-UR Navier, Université Paris-Est, France.

0008-8846/$ – see front matter © 2009 Elsevier Ltd. All rights reserved.
doi:10.1016/j.cemconres.2009.09.017

porosities, and volume fractions are changed below. This is in short the focus of this paper, which ultimately aims at linking mix proportions (w/c ratio) to microstructure (C–S–H packing densities) and mechanical phase properties. In particular, with regard to substoichiometric conditions, this research departs from the following points of inquiry:

- With regard to cement chemistry, how do substoichiometric conditions affect the amount of hydration products and gel porosity in the hardened material?
- With regard to the nanogranular morphology of C–S–H, how do substoichiometric conditions affect the packing of the C–S–H solid into characteristic C–S–H phases with distinct packing densities?
- How does heat treatment affect the amount of hydration products, their microstructure and phase properties? In fact, investigation of cement pastes prepared above the stoichiometric w/c limit shows that heat curing at 60 °C favors the formation of HD C–S–H accompanied by the formation of larger capillary pores that compensate –at constant mass of hydration products– for the densification of the C–S–H matrix [18]. Yet, little is known about the effect of heat treatment on the hydration products and microstructure below $w/c = 0.42$.

To answer these questions, five cement paste samples prepared at water-to-cement ratios from 0.15 to 0.4 with and without heat treatment are investigated using novel nanoindentation techniques [29] that allow a determination of the mechanical phase properties, volume fractions and packing density distributions of highly heterogeneous materials.

2. Materials and methods

2.1. Materials

Cement pastes were prepared using an alite rich CEM 1 cement from Le Teil (for the composition, see Table 1), at five water-to-cement mass ratios, ranging from $w/c = 0.15$ to $w/c = 0.40$. The fineness of this cement is 2940 cm^2/g, and the average particle diameter, determined from laser granulometry, is 6.6 μm. Five samples prepared at $w/c = 0.15$, 0.20, 0.30, 0.35, and 0.40 were cast and cured at 20 °C in cylinder plastic tubings of 10 mm diameter and a few centimeter length. Five other samples prepared at $w/c = 0.15$, 0.20, 0.25, 0.30, and 0.35 were subject, at a material age of 48 h, to a 48 h heat treatment at 90 °C. Both series (without heat treatment and with heat treatment) were kept in the sealed tubings until testing.

2.2. Sample preparation

There are three primary goals of the surface preparation procedure for nanoindentation: (1) to achieve as flat a surface as possible, (2) to obtain repeatable results, and (3) to minimize the sample disturbance. The procedure described here is optimized to satisfy these three goals [30]:

- The first step is to trim the sample to an appropriate size using a diamond saw. Specimens were cut into 3–8 mm thick disks of 10 mm diameter (using as a cutting fluid n-decane), and then mounted on a stainless steel AFM specimen disk (Ted Pella) using a thin layer of cyanoacrylate as an adhesive.
- The second step is a coarse grinding step. The goal of this step is to make the top of the sample parallel with the bottom of the specimen disk, so there is no tilt to the surface during indentation. The sample is placed in the specially designed jig consisting of a stainless steel outer sleeve, with an opening drilled through to match the diameter of the specimen disk. An interior cylinder fits closely inside, and rests on the back of the specimen disk to apply a light weight to the sample. Inside the jig, the sample is ground on 120 grit ZirMet (Buehler) abrasive paper. Grinding proceeds until the entire surface has been ground. Keeping the sample relatively short and wide compared to the specimen disk helps to prevent the sample from tilting and creating a convex surface. The sample and the jig are then cleaned separately, with the sample in n-decane and the jig in water, in an ultrasonic bath for 5 min.
- The third and final step is the polishing step. A TexMet P (Buehler) pad, a hard, perforated, non-woven pad is mounted to a lapping wheel. The hardness of the pad assures that the highest surfaces of the sample are removed first, and the perforation gives a place for the polishing residue to collect without interfering with the polishing itself. This is particularly important because the described polishing process does not include any ongoing cleaning of the pad. The TexMet P pad is charged with approximately 0.5 mL of 1 micron oil-based diamond suspension (Metadi, Buehler). A polishing fluid helps to dissipate any heat build-up, and the oil-base specifically helps to prevent any further hydration and change in water–cement ratio. Using only one size of diamond suspension aids in the repeatability of the procedure, as there is no need for the extensive cleaning which would be required if the sample were polished by a series of smaller and smaller diamond suspensions. While this may result in a longer polishing time, it requires much less operator intervention and therefore increases the repeatability of the procedure. The sample and jig are held on the pad, approximately 3 to 4 cm from the center of the lapping wheel, and the jig is allowed to freely rotate. The wheel is then spun at 1 cycle/s, so a typical velocity underneath the sample is 18 to 25 cm/s. The relatively slow lapping speed is essential in minimizing the sample disturbance and creating a smooth surface. This polishing lasts for approximately 8 h. As before, the sample and the jig are then cleaned separately, with the sample in n-decane and the jig in water, in an ultrasonic bath for 5 min.

The above surface preparation technique consistently gave RMS roughness below 20 nm for cement pastes and enables to obtain repeatable nanoindentation results [30]. Mechanical properties measured by nanoindentation on the surface of a cement paste that has been well polished yields mechanical properties that are those of the bulk materials [31].

Table 1
Composition of the cement from Le Teil of Lafarge in mass percentage of each component provided by the manufacturer.

CaO	SiO_2	Al_2O_3	Fe_2O_3	SO_3	LOI
67.17	22.14	3.12	2.51	2.13	1.68

Alite	Belite	Ferrite	Aluminate	Anhydrite	Gypsum	Calcite
71.1	15.0	7.0	1.2	1.4	1.2	1.8

Components with a mass percentage smaller than one percent are not included.

2.3. Nanoindentation Technique

Nanoindentation consists of making contact between a sample and an indenter tip of known geometry and mechanical properties, followed by a continuously applied and recorded change in load, P, and depth, h. A typical indentation test then consists of a constantly increasing load, followed by a short hold and then a constant unloading; a P–h curve is reported. The analysis of the P–h curve proceeds by applying a continuum scale model to derive an indentation modulus, M, and a hardness, H:

$$M = \frac{\sqrt{\pi}}{2}\frac{S}{\sqrt{A_c}} \tag{1}$$

$$H = \frac{P}{A_c} \tag{2}$$

where $S = \frac{dP}{dh}|_{h=h_{max}}$ is the (measured) initial slope of the unloading branch of the P–h curve, P is the (measured) maximum indentation load, and A_c is the projected contact area of the indenter on the sample surface. Using the Oliver and Pharr method, the projected contact area, A_c, is determined as a function of the (measured) maximum indentation depth, h_{max} [32]. The samples were tested with a CSM Nanoindentation Tester (CSM Instruments, Peseux, Switzerland) at MIT, Cambridge, MA, using a diamond Berkovich tip.

Recognizing the high heterogeneity of cement paste at the nano- and micro-scale, applying the indentation technique is a challenge, as it is difficult to choose to indent on a specific material phase with sufficient repeatability. To address this challenge, it is advantageous to perform large grids of indentations on heterogeneous samples, such as cement paste [21,23,24], and other composite materials [33,34]. Then, if the grid size and indentation depth are chosen properly, each indentation test may be treated as an independent statistical event; and a subsequent statistical deconvolution of the indentation results can be applied. Since the nanoindentation technique only provides mechanical information, the subsequent statistical analysis, called the deconvolution technique, only makes a distinction between 'mechanical phases', i.e., to volumes of matter with distinct mechanical properties. From now on we will refer to a 'mechanical phase' or 'mechanically activated phase' as a 'phase', characterized by a mechanical homogeneity, independent of its chemical composition or of its chemical heterogeneity.

2.3.1. Preliminary considerations

Since the statistical indentation technique came recently under scrutiny [35][2], it is useful to briefly recall the focus of the technique and its ingredients. The use of relations (1) and (2) to link indentation quantities to constitutive properties is based on the infinite homogeneous half-space model. In the case of a heterogeneous material, such a homogeneous response can be viewed as an asymptotic case for indentation modulus M, provided that the elementary size of the heterogeneity D (for instance clinker in cement paste) is much larger than the indentation depth; typically $h/D<1/10$. For hardness, from simulations of conical indentations on (almost) rigid perfectly plastic biphasic systems considering different inclusion phases (particle embedded in a matrix, thin film on a substrate), Durst et al. [37] concluded that $h/D<\min(1/4;1/2\tan\theta)$ (where $\theta=70.32°$ is the equivalent cone angle representative of the Berkovich indenter) was sufficient to measure correctly the indentation hardness (and thus strength properties) of the inclusion phase. This means that the material volume solicited elastically below the indenter is much larger than the volume solicited plastically. These studies provide an upper bound for the indentation depth in view of the assessment of mechanical properties based on continuum scale models from which Eqs. (1) and (2) derive. A lower bound for the indentation depth is provided by the scale separability condition of continuum models, meaning that the indentation depth which defines the characteristic length scale of strain and stress variations below the indenter must be much larger than the characteristic size of the elementary heterogeneity; for instance in the case of the C–S–H gel, the characteristic particle size of 3–5 nm [18]. Finally, one could add surface roughness to the set of length scales that delimit the upper bound of the indentation depth. In order to approach most the ideal configuration of an infinite half-space with a flat surface, the indentation depth should be greater than the roughness. For cement paste nanoindentation, this aspect has been addressed by Miller et al. [30] and led to the development of a surface preparation protocol outlined here above. Given the multiphase nature of cement pastes even at microscales, these scale separability conditions are satisfied on average in our studies through force-driven nanoindentation tests operated to a maximum indentation force of $P_{max}=2$ mN, which entails a mean indentation depth of ~200 nm for all tested materials. On a selected number of materials, we also carried out micro-indentation tests with a four times higher indentation force, $P_{max}=8$ mN, which entails a mean indentation depth of 20 μm. In contrast to nanoindentation tests, micro-indentation tests do not probe phase properties, but are found to reproduce composite properties, as shown and discussed for cement paste in Ref. [23] and for other composite materials in Ref. [34].

[2] For a detailed discussion of strength and limits of statistical indentation method, see also Ref. [36].

2.3.2. Deconvolution technique

Given the multiphase nature of cementitious materials, the key to the determination of phase properties in the grid-indentation technique is the identification of the statistical distribution of the phases. This requires a deconvolution of the heterogeneous data, hence the name 'deconvolution technique'. In its original development [23,24,33], the deconvolution technique was carried out manually by fitting a number of probability density functions (PDF) to the experimental frequency plot (normalized histogram) of the measured quantity; which makes the deconvolution results dependent on the operator and his/her choice of the bin size. An improvement to automatize this process was proposed in Ref. [29] for cement paste nanoindentation and validated for other composite materials in Ref. [34], in which the phase deconvolution is done using the cumulative distribution function (CDF) rather than its derivative, the PDF. In both cases, the key to the determination of phase properties in the grid-indentation technique is the identification of the statistical distribution of the phases. This requires choosing *a priori* the type of distribution functions to deconvolute the data. We briefly recall that a distribution function is uniquely defined by its statistical moments [38]: The first moment about the origin is the mean; the second moment around the mean is the variance s^2, where s is the standard deviation; the third standardized moment, usually written as γ_1, is the skewness and is a measure of the asymmetry of the distribution function (a symmetric distribution function verifies $\gamma_1=0$; a log-normal distribution has a positive skewness); and so on. If the measurements and the material were perfect, for infinitely shallow indentations one would expect the peaks to be infinitely sharp (Fig. 1a). In this case, each peak would be characterized by its first moment (mean value) only. Practically however, there are several reasons for which the peaks of the histogram are not infinitely sharp, requiring the use of moments of higher order. To name a few: the measurements exhibit some noise. The noise is considered as random and creates a spread of the peaks, but no asymmetry (Fig. 1b). Furthermore, each phase has its own intrinsic variability, which also creates a spread of the peaks (Fig. 1b). It may well be that, as a result of its processing, the material has a distribution function of its properties within each phase which is asymmetric. Nevertheless, in an *a priori* analysis, with no further information available on processing, it is not possible to justify an asymmetric distribution of the properties in each phase. In addition, even for an ideal material and ideal measurements, due to their finite depth some indentations will solicit mechanically two (or more) phases simultaneously, and the measured property will be a composite property. Quantifying the composite response is complicated, since it is the result of a three-dimensional interaction between the indenter probe and the phases probed. Nevertheless we can assert that the composite response must be bound by the values of the individual peaks (see Fig. 1c). As a result, the finite depth of the indentation introduces some asymmetry: The lowest peak is better characterized by a positive skewness, $\gamma_1>0$; and the highest peak with a negative skewness $\gamma_1<0$. Yet, such an analysis would depend on the observer. Thus, in order to automatize the deconvolution process, we choose to characterize all peaks with only one model-phase distribution, with non-zero first and second moments (mean and variance) and a zero skewness $\gamma_1=0$. For the sake of simplicity, the distribution is chosen so that all standardized central moments of higher order are zero. This distribution is the Gaussian distribution.

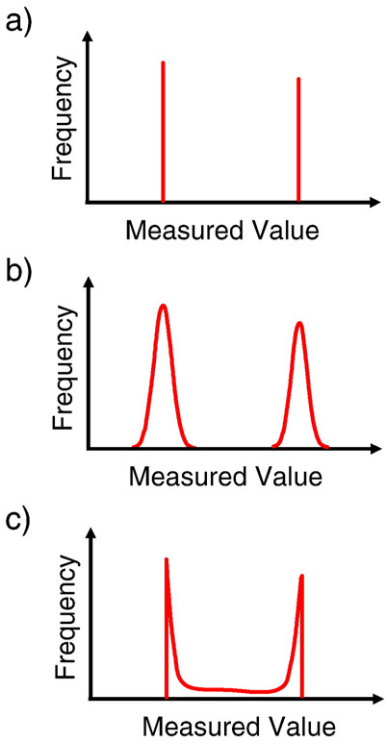

Fig. 1. Expected frequency plots for a biphasic material. (a) Perfect measurements and materials and infinitely shallow indentations; (b) Imperfect measurements or material and infinitely shallow indentations; (c) Perfect measurements and material and indentations with finite depth.

The deconvolution technique then consists of fitting the experimental cumulative distribution function (CDF) of the measured indentation modulus M and indentation hardness H, to the sum of model-phase CDFs [29,34]:

$$\min \sum_{i=1}^{N} \sum_{X=(M,H)} \left(\sum_{j=1}^{n} f_j D(X_i; \mu_j^X, s_j^X) - D_X(X_i) \right)^2 \quad \text{s.t.} \quad \sum_{j=1}^{n} f_j = 1 \tag{3}$$

where $D_X(X_i)$ are the experimental CDFs generated from N indentation tests performed on a specimen surface:

$$D_X(X_i) = \frac{i}{N} - \frac{1}{2N};\ \text{for } i \in [1;N];\ X = (M,H) \tag{4}$$

f_j stands for the surface fraction that each phase $j=1,n$ occupies of the indented surface. In an *a priori* analysis (as discussed here above), the best choice for the distribution of the mechanical properties of each phase is the Gaussian distribution, identified by its mean value μ_j^X and its standard deviation s_j^X. The CDF of the j-th Gaussian distributed phase is given by:

$$j = 1,n; D(X_i; \mu_j^X, s_j^X) = \frac{1}{s_j^X \sqrt{2\pi}} \int_{-\infty}^{X_i} \exp\left(\frac{-(u-\mu_j^X)^2}{2(s_j^X)^2} \right) du;\ X = (M,H) \tag{5}$$

Finally, to ensure that phases have sufficient contrast in properties, and thus to avoid the overlap of two neighboring Gaussians, the optimization problem is additionally constrained by:

$$\mu_j^X + s_j^X < \mu_{j+1}^X - s_{j+1}^X,\ X = (M,H) \tag{6}$$

The results of the deconvolution technique are estimates of the $n \times 5$ unknowns $\{\mu_j^M, s_j^M, \mu_j^H, s_j^H, f_j\}$, $j=1,n$; that is, the mean and standard deviation of indentation modulus and hardness for each mechanical phase, and the surface fraction. For a perfectly disordered material, which is the case of cement paste [29], surface fractions and volume fractions are identical, which is known at the Delesse principle [39]. It should be noted that the deconvolution technique is carried out here simultaneously for the two indentation quantities, M and H, the first relating to the elasticity, the second to the strength properties of the indented phases. Given the difference in material volume solicited respectively elastically and plastically, as discussed above, this consideration adds some robustness to the technique that strongly aids the identification of mechanically activated material phases by grid-indentation. For instance, it avoids the identification of spurious peaks as mechanically activated material phases.

By way of illustration, Fig. 2 shows the results of the deconvolution technique in terms of both CDFs and PDFs for indentation modulus and indentation hardness for the $w/c=0.4$ cement paste. The CDFs and PDFs show the presence of four phases in the hardened material system, which by their phase values can be identified from left (soft) to right (hard) as:

1. Low-Density C–S–H (LD C–S–H), characterized by a phase modulus $M=22.5\pm5.0$ GPa ($\mu_1^M \pm s_1^M$), and a phase hardness $H=0.61\pm0.17$ GPa ($\mu_1^H \pm s_1^H$). In the $w/c=0.4$ system, this phase has a volume fraction of 50% (area below the first Gaussian curve in the PDF plots in Fig. 2);
2. High-Density C–S–H (HD C–S–H), characterized by a phase modulus $M=30.4\pm2.9$ GPa ($\mu_2^M \pm s_2^M$), and a phase hardness $H=0.92\pm0.10$ GPa ($\mu_2^H \pm s_2^H$), which occupies in the $w/c=0.4$ cement system a volume fraction of 18%.
3. A third mechanical phase which we label as Ultra-High-Density (UHD) phase as explained later on, characterized by a phase modulus $M=40.9\pm7.7$ GPa ($\mu_3^M \pm s_3^M$), and a phase hardness $H=1.46\pm0.45$ GPa ($\mu_3^H \pm s_3^H$). Note that these values exceed the reported nanoindentation values of LD and HD C–S–H; yet the elasticity value is close to the characteristic elasticity values of portlandite, $M=38.0\pm5$ GPa, as obtained by both nanoindentation on large CH crystals [21], and from Molecular Dynamic simulation on CH ($M=39$ GPa) [40]. While the mechanical identification of this UHD phase as portlandite remains a possibility for high w/c ratio materials, we will argue in this paper that the occurrence of this phase in substantial proportions in low w/c materials (below the stoichiometric limit) with and without heat treatment, is indicative of a C–S–H like hydration phase that possesses similar microstructural features as LD and HD C–S–H. As observed in Fig. 2, this phase is necessary in order to capture reasonably well the experimental probability density functions. It indeed occupies a volume fraction of 19% in the $w/c=0.4$ cement system, which proves its statistical significance.
4. Unhydrated clinker, characterized by a phase modulus $M=93.4\pm44.8$ GPa ($\mu_4^M \pm s_4^M$), and a phase hardness $H=6.13\pm4.22$ GPa ($\mu_4^H \pm s_4^H$). This phase occupies 14% in the hardened $w/c=0.4$ system, which provides an estimate of the hydration degree from:

$$\alpha = 1 - f_c \tag{7}$$

I.e., for the $w/c=0.4$ cement system, $\alpha=0.86$. The relatively high standard deviation of the hardest phase is commonly observed when deconvoluting grids of indentations [34]: When indenting an inclusion surrounded by a much softer matrix, there may always remain an elastic component from the surrounding matrix.

The mechanical phase properties obtained here for the $w/c=0.40$ reference material are in very good agreement with published phase properties of C–S–H [20,21,23,29] and of pure clinker properties [41].

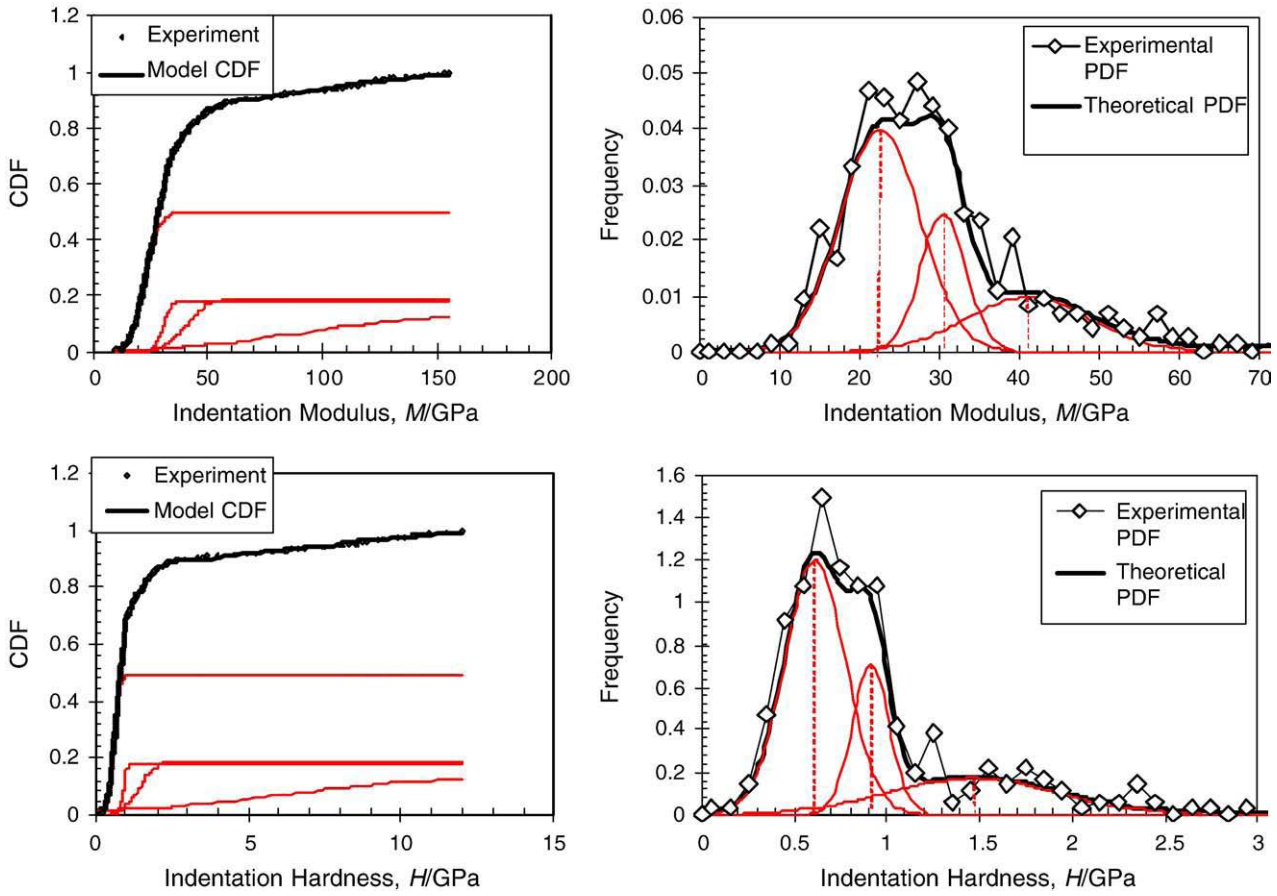

Fig. 2. Illustration of deconvolution technique for the $w/c = 0.4$ cement paste (no heat treatment): (left) Cumulative distribution functions (CDF) and (right) Probability density functions (PDF) for indentation modulus M (top) and indentation hardness H (bottom). [Deconvolution of 396 (M, H) values obtained on a grid with 20 μm grid spacing; force-driven nanoindentation tests with maximum force $P = 2$ mN, leading to an average indentation depth of 200–300 nm. For purpose of readability of the probability density functions (PDF) only the first three peaks are displayed, while CDFs show all four phases.]

2.3.3. Assessment of C–S–H packing density distribution

An additional refinement of the analysis of the nanoindentation tests of the hydration phases (Phases 1 to 3 in Fig. 2) consists in recognizing that each indentation modulus and indentation hardness obtained on the grid represents in fact a stiffness and strength composite response of a porous material composed of a hydrated solid phase and pore space [29]:

$$M_i = m_s \times \Pi_M(\nu_s, \eta_i, \eta_0) \tag{8}$$

$$H_i = h_s \times \Pi_H(\alpha_s, \eta_i, \eta_0) \tag{9}$$

where $m_s \to \lim_{\eta=1} M$ and $h_s \to \lim_{\eta=1} H$ are the asymptotic particle contact stiffness and contact hardness, respectively, that relate to the solid's Young's modulus E_s, Poisson's ratio ν_s, cohesion c_s and friction coefficient α_s by [22,23,42–44]:

$$m_s = \frac{E_s}{1-\nu_s^2} \tag{10}$$

$$h_s = c_s \times A(1 + B\alpha_s + (C\alpha_s)^3 + (D\alpha_s)^{10}) \tag{11}$$

where $A = 4.76438$, $B = 2.5934$, $C = 2.1860$, and $D = 1.6777$. Furthermore, η_i is the solid fraction or packing density ('one minus porosity'), and η_0 is the solid's percolation threshold, that is the solid fraction required to provide a continuous force path through the system. Above a packing density of $\eta \approx 0.6$, the influence of particle size on mechanical properties was found to be negligible [45], so that hydrated matter of cement paste – from a mechanical point of view – appears to possess a very distinct disordered morphology of the solid phase, similar to a polycrystal, characterized by a solid percolation threshold of $\eta_0 \simeq 1/2$, below which the solid has no appreciable strength or stiffness [23]. For such a disordered porous material system, linear micromechanics provides the dimensionless elasticity scaling relation $\Pi_M \in [0,1]$. This relation exhibits very little sensitivity to the Poisson's ratio of the solid phase, ν_s, and can therefore be well approximated by its expression for $\nu_s = 0.2$, for which Eq. (8) reduces to a linear scaling of the indentation modulus with the packing density:

$$\Pi_M(\nu_s = 0.2, \eta_i, \eta_0 = 1/2) = 2\eta_i - 1 \geq 0. \tag{12}$$

Based on non-linear micromechanics [46], similar relations were recently developed for the scaling $\Pi_H \in [0,1]$ of the indentation hardness with the packing density [43,44]:

$$\Pi_H(\alpha_s, \eta_i, \eta_0 = 1/2) = \Pi_1(\eta_i, \eta_0) + \alpha_s(1-\eta) \times \Pi_2(\alpha_s, \eta_i, \eta_0) \tag{13}$$

where:

$$\Pi_1(\eta_i, \eta_0) = \frac{\sqrt{2(2\eta-1)} - (2\eta-1)}{\sqrt{2}-1} \times (1 + a(1-\eta) + b(1-\eta)^2 + c(1-\eta)^3) \tag{14}$$

$$\Pi_2(\alpha_s, \eta_i, \eta_0) = \frac{2\eta-1}{2}(d + e(1-\eta) + f(1-\eta)\alpha_s + g\alpha_s^3) \tag{15}$$

and where $a = -5.3678$, $b = 12.1933$, $c = -10.3071$, $d = 6.7374$, $e = -39.5893$, $f = 34.3216$ and $g = -21.2053$ are all constants associated

with a Berkovich indenter geometry and a polycrystal morphology with percolation threshold of $\eta_0 = 1/2$.

These scaling relations are a versatile tool to probe the microstructure sensed by the large array of grid-indentation tests. [Details of the method, validation and application to C–S–H, clays and bones can be found in [29]]. In a forward application, use of the scaling relations (8) and (9) requires knowledge of four solid properties (m_s, ν_s,c_s,α_s) and of the solid's packing density η to determine the composite indentation quantities M and H. In an inverse application, $N \geq 3$ indentation tests are required to determine from experimental (M, H) values the solid properties (m_s,c_s,α_s) and the solid's packing density η_i for each grid point. In particular, it is possible to back-calculate from $N \geq 3$ tests in which $(M, H)_i$ is measured the packing density η_i for each grid point and determine the packing density distributions of the hydration phases in the hardened material system using a similar deconvolution method as for (M, H). Finally, an additional outcome of the packing density distribution is an estimate of the gel porosity, from:

$$\varphi_0 = \sum_{j=1}^{n'} f_j (1 - \eta_j) \tag{16}$$

where $n' = 3$ is the number of hydration phases (see Fig. 2), f_j is the volume fraction of each hydration phase, determined from the deconvolution, and η_j the corresponding mean phase packing density. In return, in the absence of true macro-capillary pores, the total porosity (i.e. pore volume divided by total volume) is obtained by multiplying the gel porosity with the hydration degree as defined by Eq. (7):

$$\phi_0 = \alpha\varphi_0 = \alpha \sum_{j=1}^{n'} f_j (1 - \eta_j) \tag{17}$$

At this macroscopic scale, the total material volume is composed of the unhydrated clinker, f_c, the total porosity ϕ_0, and the total volume of solid hydration products:

$$f_h = \alpha \sum_{j=1}^{n'} f_j \eta_j = \alpha - \phi_0 \tag{18}$$

By way of illustration, Fig. 3 displays the scaling of indentation modulus M and hardness H with the packing density η for the $w/c = 0.4$ reference material together with the deconvolution of the packing density in form of packing density distribution plots, CDF and PDF. The mean relative error of the backanalysis of the packing density from M and H is $\bar{e}_M = -1.0\%$, and $\bar{e}_H = -0.7\%$, respectively; and the standard deviation of the relative error, which is a measure of the data dispersion, is $\overline{e}_M = 10.1\%$ for indentation modulus and $\overline{e}_H = 9.0\%$ for indentation hardness. In the backanalysis we fixed the value of $m_s = 65$ GPa, on the basis of atomistic simulation results [47,48]. In turn, we obtain the particle strength properties $h_s = 3.22$ GPa, $\alpha_s = 0.181$, which translate into a particle cohesion $c_s = 0.44$ GPa and a particle-to-particle friction angle $\varphi = \arcsin\sqrt{3\alpha^2/(3-\alpha^2)} \approx \alpha + O(\alpha^3) = 10.5^\circ$ (for details, see

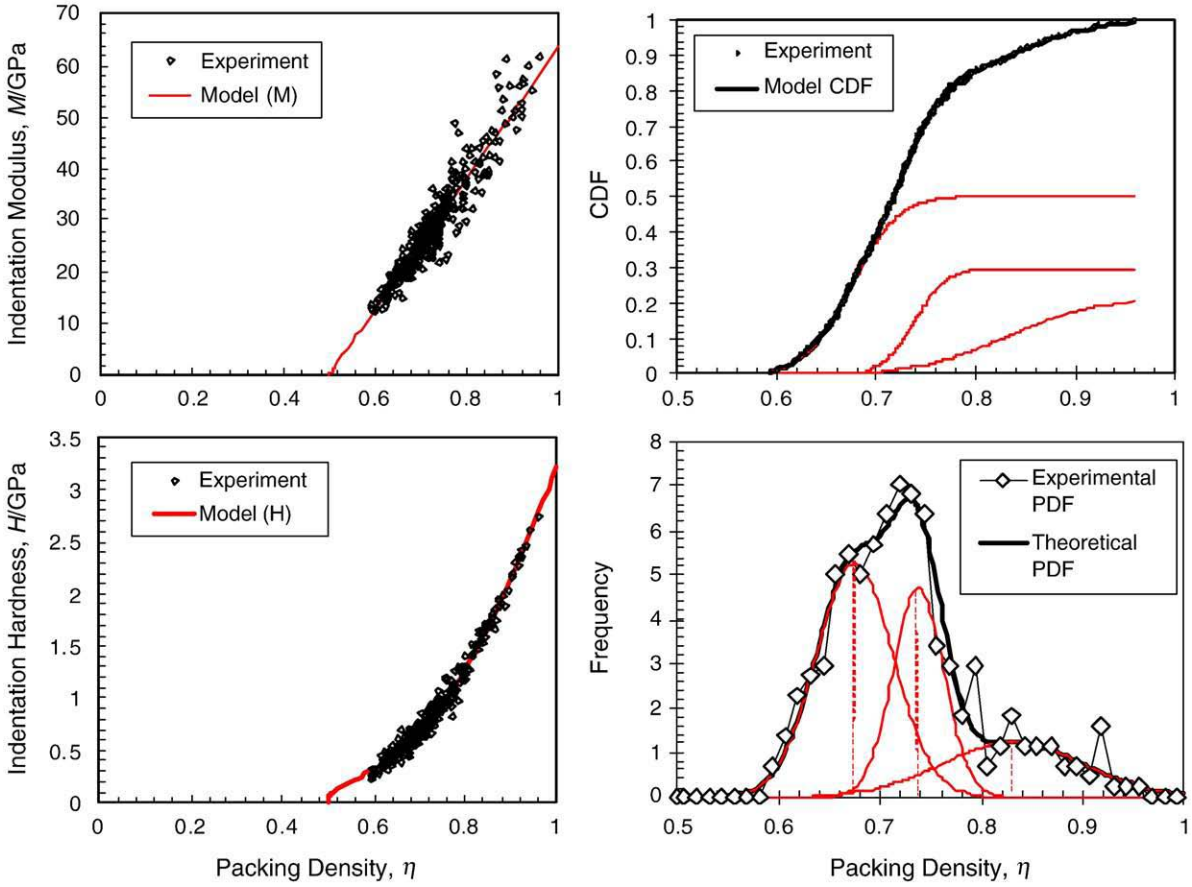

Fig. 3. Scaling of indentation modulus M and hardness H with the C–S–H packing density for the $w/c = 0.4$ material: (left) Scaling relations, (right) Packing density distributions: CDF (top), PDF (bottom). [Results for 352 (M,H) values representing hydration phases.]

Table 2
Statistical nanoindentation procedure.

Step	Description	Results
1	Deconvolution of all $(M;H)_i, i=1, N_{tot}$ with $n=4$ Gaussian distributions	Phase properties: $\{\mu_j^M, s_j^M, \mu_j^H, s_j^H, f_j\}$, $j=1,4$
2	$(M;H)$–η scaling of $(M;H)_i$, $i=1, N_{hyd}$ which satisfy $(M;H)\leq(65;3)$GPa, representative of hydration phases	Particle properties: (m_s, c_s, α_s) Packing Density: $\eta_i, i=1, N_{hyd}$
3	Deconvolution of $(M;H;\eta)_i$, $i=1, N_{hyd}$ with $n'=3$ Gaussian distributions	Hydration phase properties: $\{\mu_j^M, s_j^M, \mu_j^H, s_j^H, \mu_j^\eta, s_j^\eta, f_j\}$, $j=1,3$
4	Ensure consistency of μ_j^M, μ_j^H obtained in Step 1 and Step 3.	

[23,42–44]). Finally, the packing density distributions in Fig. 3 faithfully translate mechanical nanoproperties of the hydration phases into characteristic packing densities of the main hydration phases, namely, from left (low packing) to right (high packing) in Fig. 3:

1. The LD C–S–H phase in the $w/c=0.4$ material is found to have a characteristic particle packing density of $\eta=68\%\pm4\%$ ($\mu_1^\eta\pm s_1^\eta$), which is close to the LD C–S–H packing density one can calculate from reported density values of the C–S–H particle, $\eta_{LD}=65\%$ [17,18,29,49]. The value remains remarkably close to the random limit packing density of spheres of $\eta\approx64\%$ [26,27]. This result is surprising since SEM observations show that C–S–H is not made of monosized spherical particles. On the other hand, it has been shown that the effect of particle shape is negligible above a packing density of ~60% [45]. Within the $w/c=0.4$ material, this LD C–S–H phase constitutes 50% of all hydration products.
2. The HD C–S–H phase here has a characteristic packing density of $\eta=74\%\pm2\%$ ($\mu_2^\eta\pm s_2^\eta$), which coincides with the ordered face-centered cubic (fcc) or hexagonal close-packed (hcp) packing of $\eta=\pi/\sqrt{18}\approx74\%$ [28]. The value is consistent with reported HD C–S–H packing density values estimated from C–S–H density measurements, $\eta_{HD}=73\%\pm5\%$ [17,18,29,49]. Within the $w/c=0.4$ material, this HD C–S–H phase constitutes 29% of all hydration products.
3. The UHD phase in the $w/c=0.4$ material is characterized by a particle packing density of $\eta=83\%\pm7\%$ ($\mu_3^\eta\pm s_3^\eta$), representing 21% of all hydration products (19% of all tests when clinker phases are included).

Last, application of Eqs. (16), (17) and (18) to the $w/c=0.4$ material yields a gel porosity of $\varphi_0=27\%$, a total porosity (relative to the entire material, C–S–H plus unhydrated materials) of $\phi_0=\alpha\varphi_0=24\%$, and a solid volume fraction of the hydration products of $f_h=65\%$.

In addition to the deconvolution of all indentation results, the deconvolution of the hydration phases will be applied to each series of tests, for all indentation results in which $M<65$ GPa and $H<3.0$ GPa, which is indicative of a hydration phase. Indentation results $M>65$ GPa and $H>3.0$ GPa are representative of residual clinker phases or of a composite response of clinker phases with hydration products. The number of tests into the hydration phases over the total number of tests provides a second estimate of the hydration degree, in addition to Eq. (7). In what follows we will report both values, while working with the average of both values in the interpretation of the results.

Table 2 summarizes the statistical nanoindentation technique procedure.

3. Nanoindentation results

3.1. Deconvolution results

Table 3 summarizes the results of the deconvolution procedure of the materials hydrated at 20 °C. The results show a fair amount of consistency with previous reported results of cement pastes in terms of phase properties and particle properties, and show that the main

Table 3
(M, H) Deconvolution results of non-heat treated materials.

	w/c	0.15		0.20		0.30		0.35		0.40	
	N_{tot}/N_{hyd}[a]	292	166	697	481	726	577	275	227	396	352
Peak		μ	s	μ	s	μ	s	μ	s	μ	s
1	M_1/GPa	–	–	19.4	4.8	21.9	4.9	25.6	3.5	22.5	5.0
	H_1/GPa	–	–	0.44	0.23	0.58	0.12	0.60	0.10	0.61	0.17
	η_1	–	–	0.62	0.02	0.68	0.03	0.71	0.02	0.68	0.04
	f_1[b]	0.0 (0.0)		0.02 (0.03)		0.27 (0.30)		0.37 (0.47)		0.50 (0.50)	
2	M_2/GPa	27.7	5.7	31.8	6.1	31.3	4.5	32.0	2.9	30.4	2.9
	H_2/GPa	0.74	0.11	0.88	0.21	0.87	0.17	0.87	0.17	0.92	0.10
	η_2	0.69	0.07	0.75	0.04	0.75	0.04	0.75	0.03	0.74	0.02
	f_2	0.0 (0.03)		0.50 (0.74)		0.35 (0.52)		0.30 (0.35)		0.18 (0.29)	
3	M_3/GPa	41.1	8.1	46.1	8.3	44.2	8.4	43.6	8.6	40.9	7.7
	H_3/GPa	1.15	0.33	1.67	0.34	1.50	0.46	1.49	0.45	1.46	0.45
	η_3	0.82	0.06	0.85	0.06	0.83	0.06	0.83	0.06	0.83	0.07
	f_3	0.55 (0.97)		0.17 (0.23)		0.17 (0.19)		0.13 (0.18)		0.19 (0.21)	
4	M_4/GPa	105.2	33.0	107.1	34.3	113.4	35.5	86.4	34.2	93.4	44.8
	H_4/GPa	6.62	2.58	7.09	3.10	6.79	3.16	5.04	2.92	6.13	4.22
	f_4	0.45		0.31		0.20		0.21		0.14	
Gel porosity, φ_0		0.18		0.23		0.26		0.26		0.27	
Hyd. degree, α		0.59		0.70		0.80		0.84		0.90	
Tot. porosity, ϕ_0		0.10		0.16		0.21		0.21		0.24	
Solid hyd. prod, f_h		0.49		0.54		0.60		0.62		0.65	
Unhyd. clinker, f_c		0.41		0.30		0.20		0.17		0.11	
m_s/GPa[c]		63.5		63.5		63.5		63.5		63.5	
h_s/GPa		2.69		2.99		2.98		3.06		3.22	
c_s/GPa		0.49		0.45		0.44		0.21		0.44	
α_s		0.062		0.138		0.151		0.444		0.181	

[a] Number of tests/number of tests in hydration phases.
[b] Volume fraction from deconvolution with $n=4$ phases. In-between parenthesis (…): Volume fraction relative to total volume of hydration products, from deconvolution with $n'=3$ phases of all data points with $M<65$ GPa, $H<3$ GPa.
[c] Value of $m_s=65$ GPa fixed.

effect of the mix proportion is on the volume fractions of the different material phases present in the hardened material.

3.1.1. Phase Properties

The difference in mean phase properties between materials prepared at different w/c ratios is typically smaller than the standard deviation of the same phase property for each material. Indeed, the coefficient of variation (stdev/mean) of the phase properties for the five materials is on average 8% for indentation modulus, 12% for indentation hardness and 3% for the packing density. This confirms, if need still be, that the phase properties sensed by nanoindentation are intrinsic material properties representing a nanomechanical signature of cement-based materials. In particular, the signature values for M and H of the three hydration phases relate to the characteristic packing of the hydration products in three packing densities, LD, HD and UHD. The scaling plots in Fig. 4(a–d) exemplify the nanogranular signature of the three hydration phases: The M–η and H–η scaling relations (Fig. 4(a,b)) show that the difference in phase properties relates to the difference in packing density of the three hydration phases. This dependence of both the elasticity and the strength behavior on the packing density translates into a characteristic M–H scaling relation (Fig. 4(c)) with a clear trend that the hardness (strength) increases faster than the indentation modulus (elasticity). The curved shape of the M–H scaling is reminiscent of macroscopic elastic modulus–compressive strength curves, which indeed may find here – at the C–S–H nanoscale – their origin. This trend is also captured in the (M/H)–η plot (Fig. 4(d)). For reference and comparison, let us note that Berkovich indentation into a continuum linear isotropic elastic half-space yields a value of $M/H = 5.6$ and that any value $M/H > 5.6$ is a measure of the plastic strength deformability of the indented material [23]. For instance, the value for the clinker phase we obtain from our data, $(M/H)_c = 16.0 \pm 0.9$, shows some plastic deformation capacity of the residual clinker phases, which is in excellent agreement with values reported for pure clinker phases [41]: $(M/H)_{C_3S} = 15.5$, $(M/H)_{C_2S} = 16.3$, $(M/H)_{C_3A} = 13.4$ and $(M/H)_{C_4AF} = 13.2$. Compared to these values, the (M/H)–η plot in Fig. 4(d) shows a consistent scaling of M/H with the packing density of the hydration phases: the loosest packed LD C–S–H phase has the highest value $(M/H)_{LD} = 40.3 \pm 3.5$, while the more densely packed hydration products exhibit lower values, $(M/H)_{HD} = 35.9 \pm 1.7$ and $(M/H)_{UHD} = 30.0 \pm 3.3$.

3.1.2. C–S–H packing density distributions

The probability density plots in Fig. 5 of indentation modulus M, indentation hardness H and packing density η compare the statistical response of two materials, $w/c = 0.4$ and $w/c = 0.2$. While the mean phase properties are not affected by lowering the w/c ratio, the distribution of the hydration phases is strongly affected by w/c: at low w/c, the high-density phases, HD C–S–H and UHD dominate over LD C–S–H, while it is the inverse at high w/c ratios.

3.1.3. Volume fractions

A refined analysis of the volume fractions is given in the plots of Fig. 6: Fig. 6(a) displays the overall volume fractions of the three chemophysical phases, clinker – C–S–H solid (vol.frac. f_h) – porosity (vol.frac. ϕ_0), while Fig. 6(b) displays the volume fractions of the LD C–

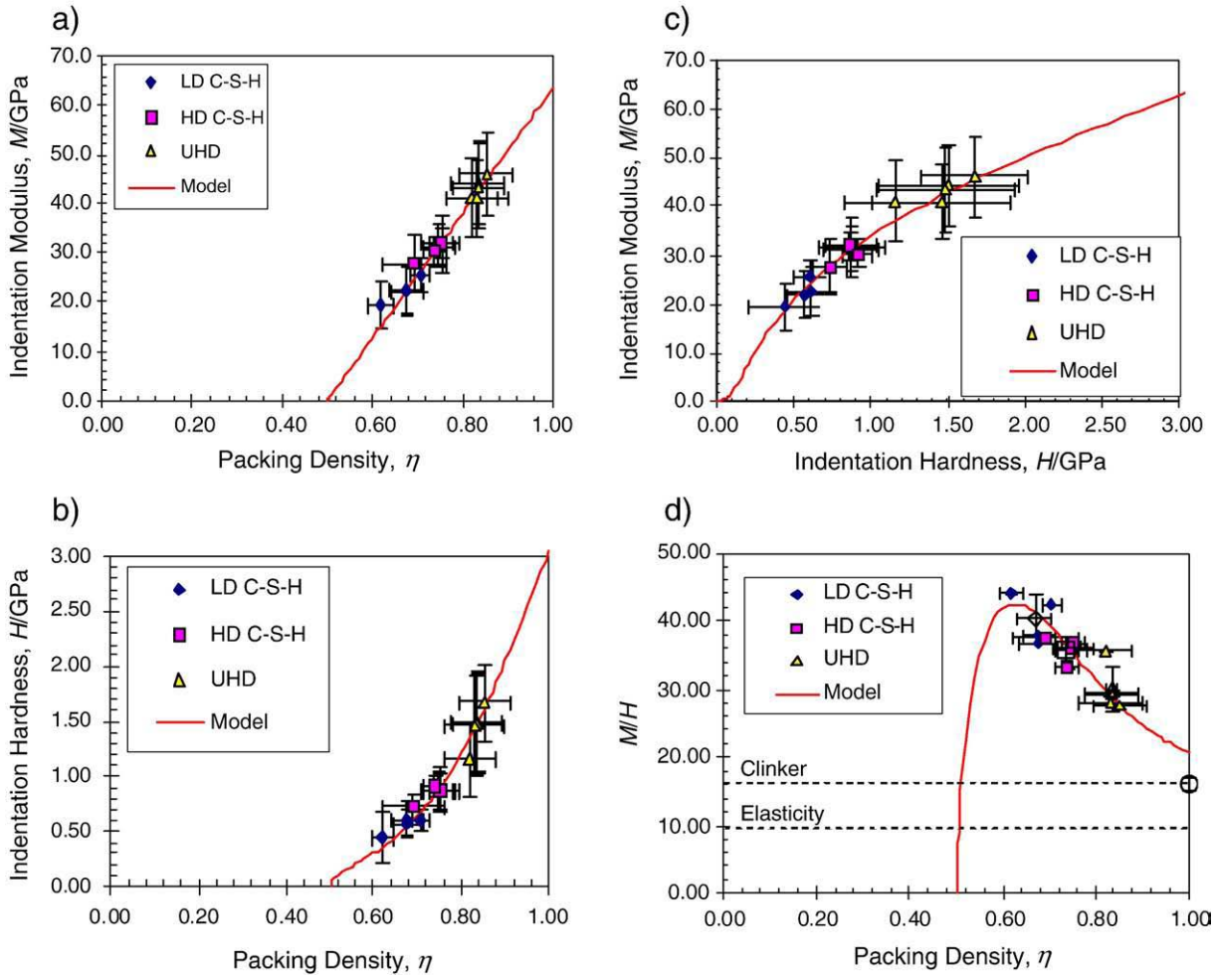

Fig. 4. The nanogranular signature of the hydration phases in low w/c materials, LD C–S–H, HD C–S–H, UHD: (a) M–η and (b) H–η scaling; (c) M–H scaling and (d) M/H–η scaling. [Results from deconvolution of five w/c materials without heat treatment.]

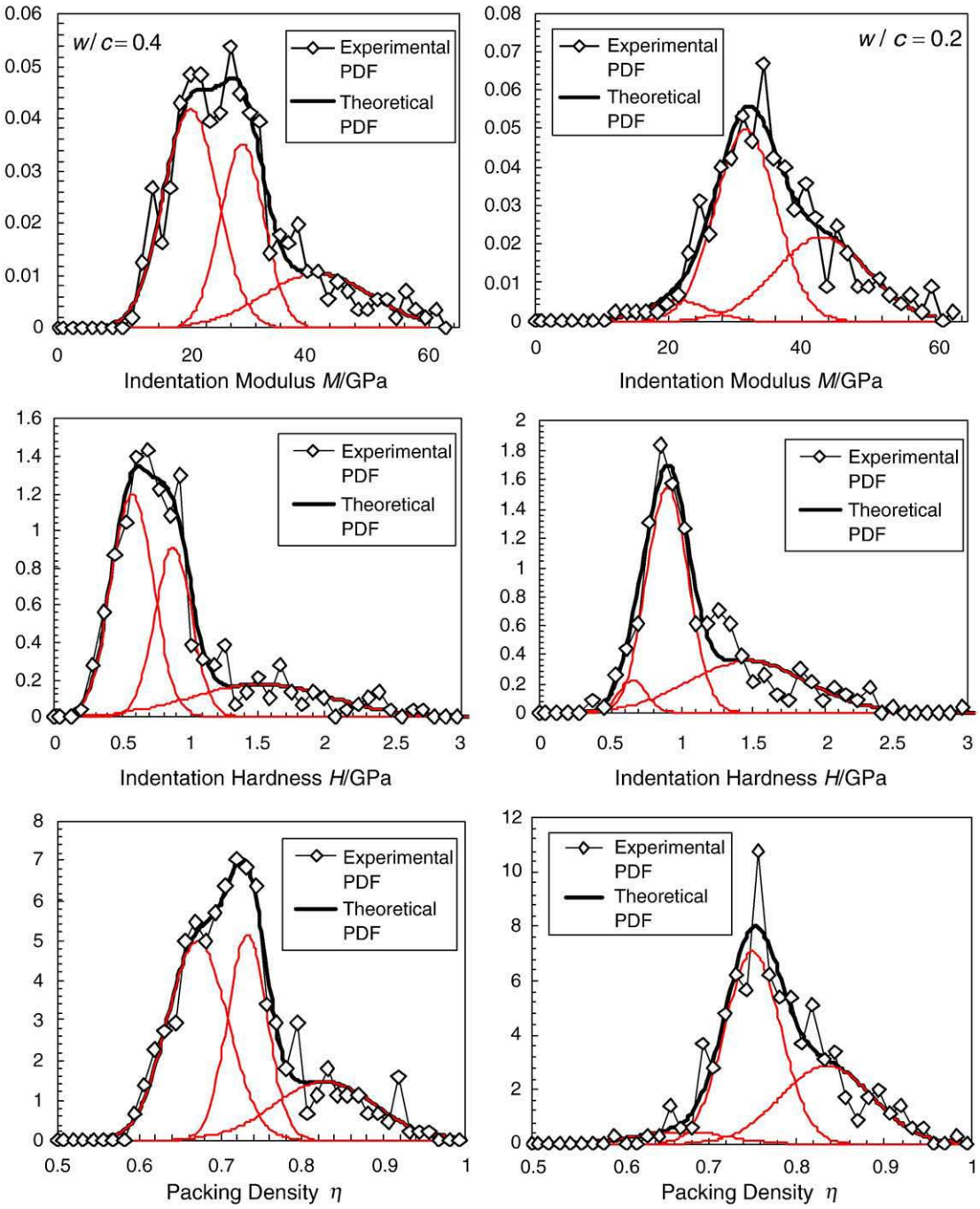

Fig. 5. PDF plots of indentation modulus, hardness and packing density of $w/c = 0.4$ (left) and $w/c = 0.2$ materials (right).

S–H, HD C–S–H and UHD phase that result from the packing of the C–S–H solid with the gel porosity. The following points deserve attention:

- As expected, the increase of the w/c ratio entails an increase in the hydration degree, $\alpha = \phi_0 + f_h$ (Fig. 6(*a*)). In turn, this increase is due to an increase in similar proportions of both the C–S–H solid (f_h) and the gel porosity ϕ_0; roughly 5% per $\Delta\,(w/c) = 0.1$ within the range $w/c \in [0.2, 0.4]$. This trend is enhanced at the lower end of the w/c spectrum, and reduced close to the stoichiometric limit.
- The increase with the w/c ratio of both the C–S–H solid and the gel porosity in similar proportions has different effects on the microstructural organization of the hydration products into LD C–S–H, HD C–S–H and UHD (Fig. 6(b)): Above $w/c = 0.2$, the volume occupied by UHD – among the hydration products – is almost constant ($f_{UHD} \simeq 20\%$), while the decrease in HD C–S–H is compensated by the formation of LD C–S–H: at low w/c, HD C–S–H dominates over LD C–S–H, while it is the inverse at high w/c ratios.
- At extremely low $w/c = 0.15$, characterized by a hydration degree on the order of $\alpha = 0.6$, a 10% gel porosity and a 50% C–S–H solid volume fraction favor (almost) exclusively the formation of the UHD phase.

In summary, while the water available for hydration increases the amount of hydration solid, it appears that the concurrent increase in gel porosity favors the formation of looser packed LD C–S–H to the detriment of HD C–S–H; while the UHD phase remains almost constant.

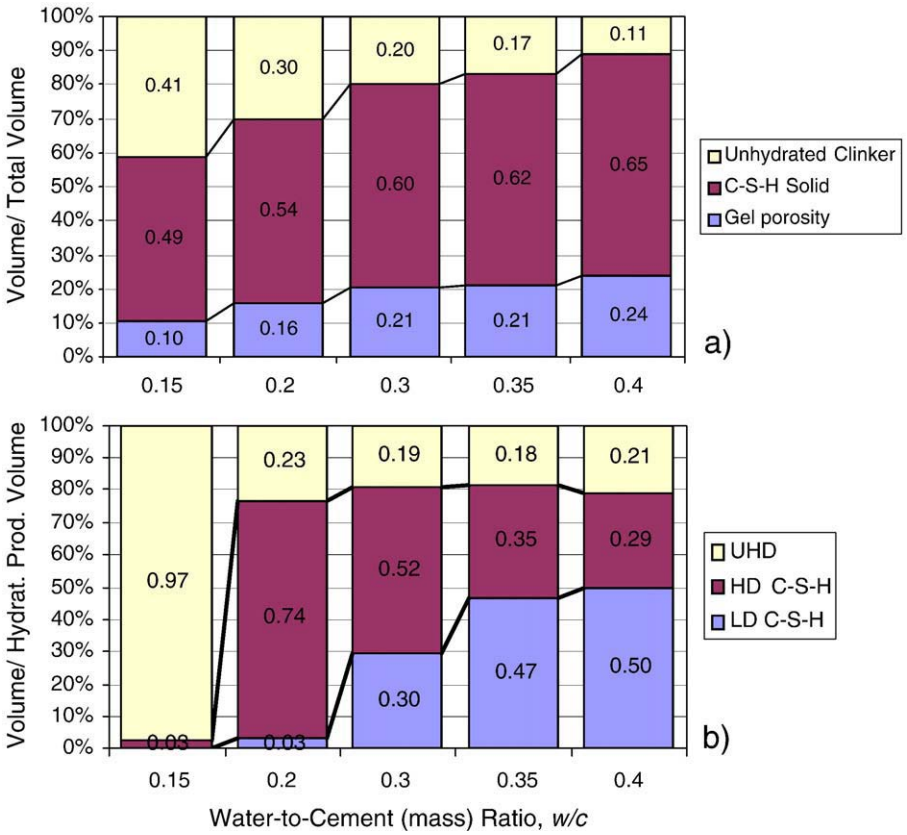

Fig. 6. Volume fraction distributions in the microstructure (without heat treatment): (a) volume fractions of the cement paste composite; (b) volume fractions of the hydration phases.

3.2. Temperature treatment

What happens to the nanogranular nature of the hydration products when the substoichiometric materials are subject, at early ages, to a heat treatment? — This question was addressed in this investigation with a second series of tests on low w/c materials that were subjected, at a material age of 2 days, to a 48 h heat treatment at 90 °C. The deconvolution results of the statistical nanoindentation campaign on this test series are given in Table 4, and the volume fractions are displayed in Fig. 7. A comparison with Table 3 and Fig. 6 readily reveals:

1. The C–S–H particle properties are not affected by the heat treatment: the particle hardness is $h_s = 2.99 \pm 0.19$ GPa without heat treatment and $h_s = 2.96 \pm 0.23$ GPa with heat treatment. This hardness is achieved respectively with a particle cohesion of $c_s = 0.41 \pm 0.11$ GPa and a friction coefficient of $\alpha_s = 0.20 \pm 0.15$ (friction angle $\varphi = 11.32° \pm 8.42°$) for the non-heat treated samples, and $c_s = 0.43 \pm 0.12$ GPa and $\alpha_s = 0.20 \pm 0.15$ (friction angle $\varphi = 9.93° \pm 6.55°$) for the heat treated samples. Otherwise said, heat treatment does not change the elementary cohesive bonds and pressure dependence of the particle-to-particle contact of the hydration products.
2. The mechanical mean phase properties of all four phases in the hardened material system are (almost) the same. For instance, averaged over the five samples in each test series, the LD C–S–H is characterized by an indentation modulus of $M_{LD} = 22.4 \pm 2.5$ GPa in the test series without heat treatment, and $M_{LD} = 19.5 \pm 3.2$ GPa in the test series with heat treatment, and similar insignificant differences between the two test series are found for all phase properties, $(M,H,\eta)_i$ i = LD,HD,UHD. This comforts our earlier suggestion that these properties are indeed intrinsic material properties that do not depend on mix proportion, heat treatment, etc.
3. Heat treatment affects the packing density distribution of the hydration products. Indeed, a comparison of Figs. 6(b) and 7(b) reveals that the application of heat treatment favors the formation of high-density phases, HD C–S–H and UHD over the entire $w/c \in [0.2,0.35]$ range. In contrast to the non-heat treated samples, for $w/c \geq 0.2$, the volume occupied by LD C–S–H – among the hydration products – is almost constant ($f_{LD} \simeq 9\%$). In turn, the volume occupied by HD C–S–H and UHD dominates the nanomechanical response of the heat treated samples. For $w/c = 0.15$, heat treatment has a negligible effect on the packing density distribution of the hydration products since already before application of the heat treatment, hydration products are almost exclusively made of UHD.
4. The gel porosity decreases by about 10% when a heat treatment is applied to samples with $w/c \geq 0.2$ (Figs. 6(a) and 7(a)), which is consistent with a densification of the hydration products. In contrast, at $w/c = 0.15$, heat treatment has no more an effect on the gel porosity.

4. Discussion

The nanoindentation results on substoichiometric cement paste materials reveal the existence of (at least) a third statistically significant phase, a ultra-high-density phase of significant proportion, which we coined UHD phase. The phase properties of this phase, $M_{UHD} = 42.8 \pm 2.3$ GPa, $H_{UHD} = 1.43 \pm 0.19$ GPa (mean ± stdev for the ten materials) are much lower than those of pure clinker [41]. The mean values of the peaks for the UHD phase and for the clinker phase are separated on average by 1.6 times the sum of the standard deviation of those same two peaks: The UHD phase and the clinker phase exhibit almost no overlap. This suggests that the UHD phase is

Table 4
(M, H) Deconvolution results of heat treated materials.

	w/c	0.15		0.20		0.25		0.30		0.35	
	N_{tot}/N_{hyd}[a]	298	172	275	191	286	216	293	237	274	214
Peak		μ	s	μ	s	μ	s	μ	s	μ	s
1	M_1/GPa	–	–	15.4	3.4	23.1	2.0	20.2	2.0	19.3	3.3
	H_1/GPa	–	–	0.26	0.10	0.74	0.10	0.53	0.10	0.41	0.10
	η_1	–	–	0.63	0.03	0.71	0.02	0.63	0.02	0.64	0.05
	f_1[b]	0.0 (0.0)		0.08 (0.13)		0.05 (0.09)		0.0 (0.02)		0.06 (0.09)	
2	M_2/GPa	–	–	23.9	2.5	32.4	3.4	30.6	6.3	27.8	5.2
	H_2/GPa	–	–	0.59	0.10	0.98	0.14	0.86	0.23	0.78	0.18
	η_2	–	–	0.70	0.02	0.76	0.03	0.74	0.04	0.72	0.04
	f_2	0.0 (0.0)		0.07 (0.13)		0.47 (0.61)		0.61 (0.73)		0.42 (0.54)	
3	M_3/GPa	42.5	9.5	39.1	9.0	44.0	8.2	46.0	9.1	41.0	8.0
	H_3/GPa	1.29	0.42	1.18	0.39	1.48	0.36	1.71	0.48	1.42	0.34
	η_3	0.83	0.07	0.82	0.05	0.85	0.04	0.85	0.06	0.82	0.05
	f_3	0.59 (1.00)		0.54 (0.74)		0.26 (0.30)		0.21 (0.25)		0.27 (0.37)	
4	M_4/GPa	115.7	27.1	107.1	39.1	116.1	22.5	110.6	28.9	92.3	43.3
	H_4/GPa	7.02	1.89	5.60	3.10	6.58	1.57	7.73	2.35	5.58	3.06
	f_4	0.41		0.32		0.22		0.18		0.25	
Gel porosity, φ_0		0.17		0.22		0.23		0.23		0.25	
Hyd. degree, α		0.58		0.70		0.77		0.82		0.80	
Tot. porosity, ϕ_0		0.10		0.15		0.17		0.19		0.19	
Solid hyd. prod, f_h		0.48		0.54		0.60		0.63		0.60	
Unhyd. clinker, f_c		0.42		0.30		0.23		0.18		0.20	
m_s/GPa[c]		63.5		63.5		63.5		63.5		63.5	
h_s/GPa		2.77		2.67		3.08		3.09		3.20	
c_s/GPa		0.49		0.27		0.58		0.41		0.38	
α_s		0.067		0.308		0.044		0.193		0.246	

[a] Number of tests/number of tests in hydration phases.
[b] Volume fraction from deconvolution with $n=4$ phases. In-between parenthesis (…): Volume fraction relative to total volume of hydrates, from deconvolution with $n'=3$ phases of all data points with $M<65$ GPa and $H<3$ GPa.
[c] Value of $m_s=65$ GPa fixed.

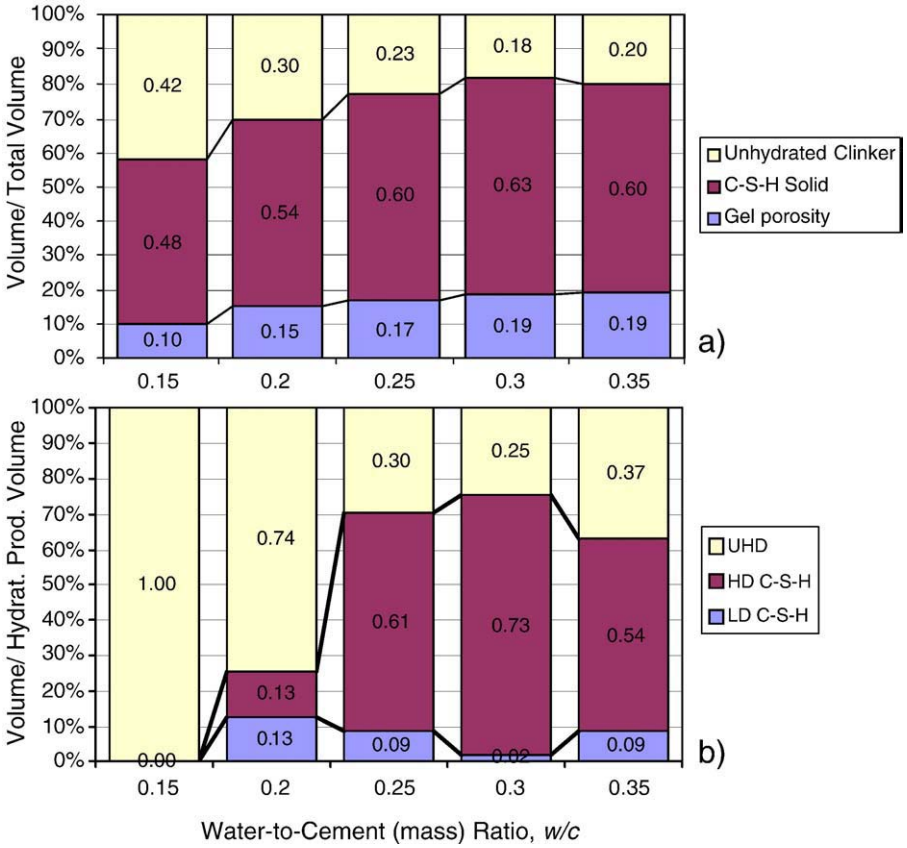

Fig. 7. Effect of heat treatment on volume fraction distributions in the microstructure: (a) volume fractions of the cement paste composite; (b) volume fractions of the hydration phases.

indeed a hydration phase. Given the closeness of the elasticity to that of CH [21,40], one could arguably make the case, for high *w/c* ratio materials, that the UHD phase could contain some CH. On the other hand, its dominance in low *w/c* materials and in particular in heat treated cement pastes suggests that this phase must be as stable vis-a-vis heat treatment as C–S–H. In fact, the phase properties of UHD appear to be affected neither by mix proportions nor heat treatment. That is, they constitute intrinsic material properties representative of a phase made of one or several hydration products. Furthermore, although the chemical composition of this phase remains unclear, its nanomechanical properties, *M* and *H*, were found to follow similar packing density scaling relations as LD C–S–H and HD C–S–H. This suggests that, as is the case for LD C–S–H and HD C–S–H, the mechanical properties of the UHD phase are governed in first order by its characteristic packing density, the chemistry being of second order. One could argue that the packing density of the UHD phase ($\eta_{UHD} = 0.83 \pm 0.01$) comes remarkably close to a two-scale random packing limit of $1-(1-0.64)^2 = 87\%$; meaning that the solid hydration products that form the UHD phase may well be of different sizes and eventually chemical compositions.

We note, however, that the developed nanoindentation approach does not allow us yet to differentiate between different chemical compositions of the nanoparticles, i.e., of the elementary building blocks. The employed approach is one that senses microstructure and identifies phases through their nanomechanical signature. That is, while the mechanical similarity with LD C–S–H and HD C–S–H suggests that the elementary building block of the UHD phase is a similar solid in terms of nanomechanical performance as in LD and HD C–S–H, the exact chemical nature of this composite remains still to be revealed. It may well contain some portlandite (CH), possibly in nanocrystalline form [9,49]. An ongoing study that combines nanoindentation with EDX measurements is expected to soon shed light on the exact chemical nature of this UHD mechanical phase [50].

It is interesting to locate these different phases in the microstructure. This can be achieved by spatially mapping the indentation results on a grid. To this end, we performed a series of 900 nanoindentations on a tightly spaced grid, with a spacing of 3 μm between nanoindents. After deconvolution of the 900 nanoindentations, to each phase (LD C–S–H, HD C–S–H, UHD) is associated an interval of packing densities deduced from (*M*,*H*)-measurements, while clinker phases are recognized by their high indentation modulus and hardness. By doing so, each specific point on the grid of nanoindentations can be associated with the phase on which the nanoindentation was performed. Such a technique provides a mapping of the C–S–H phases on the indented surface within an accuracy limited by the grid spacing. The results of this mapping are displayed in Fig. 8a for a $w/c = 0.2$ material and in Fig. 8b for a $w/c = 0.3$ material. Similar to HD C–S–H, UHD can be found (i.e. in significant amount) close to the clinker grains, forming a rim in the $w/c = 0.3$ material (Fig. 8b), or filling the space in-between highly dispersed clinker grains in the $w/c = 0.2$ material (Fig. 8a). A similar observation of a high stiffness phase in the vicinity of clinker grain was reported in Ref. [51]. Some areas of UHD are also visible far from clinker grains. Yet, one could argue that this occurrence is due to the presence of a clinker grain below the surface; a conjecture that cannot be resolved with the surface mapping technique here employed. In return, a comparison of the amount of the different C–S–H phases present in the two materials clearly shows that HD C–S–H and UHD dominate low *w/c* materials, while higher *w/c* materials are increasingly dominated by LD C–S–H.

5. Conclusions

The results of this comprehensive nanoindentation investigation of cement paste prepared at low *w/c* ratios provide strong evidence that the hydration products exist in a variety of forms that differ in first order in their packing density. In particular, we find a statistically significant Ultra-High-Density phase; in addition to the already known Low-Density and High-Density C–S–H phases.

To answer our questions initially raised, we come to the following conclusions:

1. With regard to cement chemistry, we find the obvious result that lowering the *w/c* ratio reduces the vol. fraction of hydration products. Since the hydration products contain the gel porosity, the overall gel porosity increases with increasing *w/c* ratio. At the origin of this change of the gel porosity, however, is the vol. amount of LD C–S–H, HD C–S–H and UHD; that differ – in first order – only in their packing density.

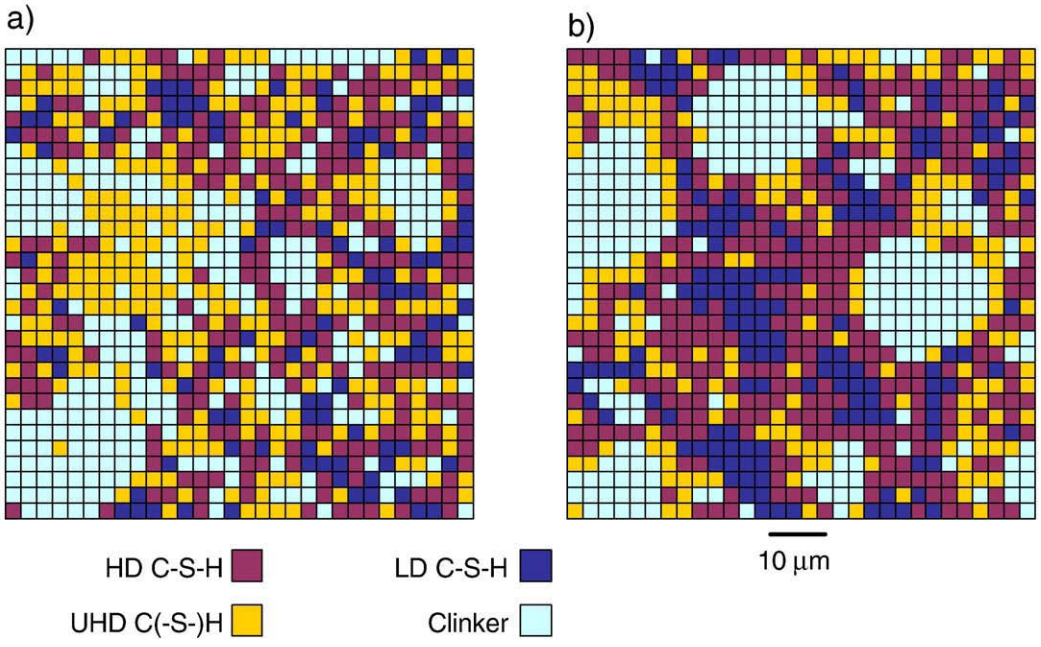

Fig. 8. Mapping of LD C–S–H, HD C–S–H, UHD and clinker phases in (a) a $w/c = 0.2$ hardened cement paste; (b) a $w/c = 0.3$ hardened cement paste.

2. With regard to the nanogranular morphology of C–S–H, LD C–S–H dominates cement-based materials prepared at high *w/c* mass ratios; HD C–S–H and UHD control the microstructure of low *w/c* ratio materials. That is, the *w/c* ratio is one parameter to monitor the packing density distribution of nanoscale C–S–H building blocks.
3. Heat treatment is another means to monitor nanoscale packing density distributions. While it has almost no effect on the amount of solid hydration products formed, nor on the hydration degree, it strongly affects the way how the solid hydrates pack to form LD C–S–H, HD C–S–H and UHD. Generally speaking, heat treatment favors the formation of denser hydration phases. This leads, in the low *w/c* materials, to a (small) reduction of the overall gel porosity.

The strong link that thus exists between microstructure and mechanical properties provides some evidence that the UHD phase is of a similar make-up –in terms of nanomechanical properties– as LD and HD C–S–H. It is expected that a combination of the here employed nanoindentation technique with advanced chemical analysis will be able, in the close future, to shed light on the exact chemical compositions of the nanoparticles, i.e., of the elementary building blocks, and to ultimately answer the still open question of how microstructure and morphology are linked to cement chemistry and reaction kinetics, and vice versa.

References

[1] T.C. Powers, T.L. Brownyard, Studies of the physical properties of hardened Portland cement paste, Bull. 22 (1947), Res. Lab. of Portland Cement Association, Skokie, IL, reprinted from U.S. J. Am. Concr. Inst. (Proc.), 43 (1947): 101–132, 249–336, 469–505, 549–602, 669–712, 845–880, 933–992.
[2] G.J. Verbeck, R.A. Helmuth, Structures and physical properties of cement paste, 5th Int. Congress Cement Chemistry, Tokyo, Japan, 1969, pp. 1–44.
[3] R.A. Helmuth, D.H. Turk, Elastic moduli of hardened portland cement and tricalcium silicate pastes: effect of porosity, Symp. Struct. Portland Cem. Paste Concr., 1966, pp. 135–144.
[4] J.H. Taplin, A method for following the hydration reaction in portland cement paste, Aust. J. Appl. Sci. 10 (1959) 329–345.
[5] B.J. Dalgleish, K. Ibe, Thin foil studies of hydrated cements, Cem. Concr. Res. 11 (1981) 729–739.
[6] H.F.W. Taylor, Studies on the chemistry and microstructure of cement pastes, Proc. Br. Ceram. Soc. 35 (1984) 65–82.
[7] H.F.W. Taylor, D.E. Newbury, An electron microprobe study of a mature cement paste, Cem. Concr. Res. 14 (1984) 565–573.
[8] K.L. Scrivener, H.H. Patell, P.L. Pratt, L.J. Parrott, Analysis of phases in cement paste using backscattered electron images, methanol adsorption and thermogravimetric analysis, Mater. Res. Soc. Symp. Proc. 85 (67–76) (1985) 1985.
[9] G.W. Groves, TEM studies of cement hydration, in: L.J. Struble, P.W. Brown (Eds.), MRS proceedings 85: Microstructural development during hydration of cement, 1987, pp. 3–12.
[10] I.G. Richardson, S.A. Rodger, G.W. Groves, The porosity and pore structure of hydrated cement pastes as revealed by electron microscopy techniques, Mater. Res. Soc. Symp. Proc. 137 (1989) 313–318.
[11] D. Viehland, J.F. Li, L.J. Yuan, Z.K. Xu, Mesostructure of calcium silicate hydrate (c–s–h) gels in portland-cement paste—a short range ordering nanocrystallinity and local compositional order, J. Am. Ceram. Soc. 79 (7) (1996) 1731–1744.
[12] J.J. Thomas, H.M. Jennings, A.J. Allen, The surface area of cement paste as measured by neutron scattering: evidence for two C–S–H morphologies, Cem. Concr. Res. 28 (6) (1998) 897–905.
[13] I.G. Richardson, The nature of C–S–H in hardened cements, Cem. Concr. Res. 29 (1999) 1131–1147.
[14] I.G. Richardson, Tobermorite/jennite- and tobermorite/calcium hydroxide-based models for the structure of C–S–H: applicability to hardened pastes of tricalcium silicate, β-dicalcium silicate, Portland cement, and blends of Portland cement with blast-furnace slag, metakaolin, or silica fume, Cem. Concr. Res. 34 (2004) 1733–1777.
[15] H.M. Jennings, A model for the microstructure of calcium silicate hydrate in cement paste, Cem. Concr. Res. 30 (2000) 101–116.
[16] P.D. Tennis, H.M. Jennings, A model for two types of calcium silicate hydrate in the microstructure of portland cement pastes, Cem. Concr. Res. 30 (2000) 855–863.
[17] H.M. Jennings, Colloid model of C–S–H and implications to the problem of creep and shrinkage, Mater. Struct. 37 (265) (2004) 59–70.
[18] H.M. Jennings, J.J. Thomas, J.S. Gevrenov, G. Constantinides, F.-J. Ulm, A multi-technique investigation of the nanoporosity of cement paste, Cem. Concr. Res. 37 (3) (2007) 329–336.
[19] H.M. Jennings, Refinements to colloid model of C–S–H in cement: CM-II, Cem. Concr. Res. 38 (3) (2008) 275–289.
[20] G. Constantinides, F.-J. Ulm, K. Van Vliet, On the use of nanoindentation for cementitious materials, Mater. Struct. 36 (3) (2003) 191–196.
[21] G. Constantinides, F.-J. Ulm, The effect of two types of C–S–H on the elasticity of cement-based materials: results from nanoindentation and micromechanical modeling, Cem. Concr. Res. 34 (1) (2004) 67–80.
[22] F.-J. Ulm, G. Constantinides, F.H. Heukamp, Is concrete a poromechanics material? — A multiscale investigation of poroelastic properties, Mater. Struct. 37 (265) (2004) 43–58.
[23] G. Constantinides, F.-J. Ulm, The nanogranular nature of C–S–H, J. Mech. Phys. Solids 55 (1) (2007) 64–90.
[24] M.J. DeJong, F.-J. Ulm, The nanogranular behavior of C–S–H at elevated temperatures (up to 700C), Cem. Concr. Res. 37 (1) (2007) 1–12.
[25] F.-J. Vandamme, F.-J. Ulm, Nanogranular origin of concrete creep, Proc. Natl. Acad. Sci. U. S. A. 106 (26) (2009) 10552–10557.
[26] H.M. Jaeger, S.R. Nagel, Physics of the granular state, Science 255 (5051) (1992) 1523–1531.
[27] A. Donev, I. Cisse, D. Sachs, E.A. Variano, F.H. Stillinger, R. Connely, S. Torquato, P.M. Chaikin, Improving the density of jammed disordered packings using ellipsoids, Science 303 (2004) 990–993.
[28] N.J.A. Sloane, Kepler's conjecture confirmed, Nature 395 (1998) 435–436.
[29] F.-J. Ulm, M. Vandamme, C. Bobko, J.A. Ortega, K. Tai, C. Ortiz, Statistical indentation techniques for hydrated nanocomposites: concrete, bone, and shale, J. Am. Ceram. Soc. 90 (9) (2007) 2677–2692.
[30] M. Miller, C. Bobko, M. Vandamme, F.-J. Ulm, Surface roughness criteria for cement paste nanoindentation, Cem. Concr. Res. 38 (4) (2008) 467–476.
[31] G. Constantinides, F.-J. Ulm, Invariant mechanical properties of calcium–silicate–hydrates (C–S–H) in cement-based materials: Instrumented nanoindentation and microporomechanical modeling. MIT-CEE Res. Rep. R06-01 (Ph.D. thesis). Massachusetts Institute of Technology, Department of Civil and Environmental Engineering, Cambridge MA, 2006.
[32] W.C. Oliver, G.M. Pharr, An improved technique for determining hardness and elastic modulus using load and displacement sensing indentation experiments, J. Mater. Res. 7 (6) (1992) 1564–1583.
[33] G. Constantinides, K.S. Ravi Chandran, F.-J. Ulm, K.J. Van Vliet, Grid indentation analysis of composite microstructure and mechanics: principles and validation, Mater. Sci. Eng., A 430 (1–2) (2006) 189–202.
[34] N.X. Randall, M. Vandamme, F.-J. Ulm, Nanoindentation analysis as a two-dimensional tool for mapping the mechanical properties of complex surfaces, J. Mater. Res. 24 (3) (2009) 679–690.
[35] P. Trtik, B. Münch, P. Lura, A critical examination of nanoindentation on model materials and hardened cement pastes based on virtual experiments, Cem. Concr. Composites 31 (2009) 705–714.
[36] F.-J. Ulm, M. Vandamme, H.M. Jennings, J. Vanzo, M. Bentivegna, K.J. Krakowiak, G. Constantinides, C.P. Bobko, K.J. Van Vliet, Does microstructure matter for statistical nanoindentation techniques? Cem. Concr. Composites (in press). doi:10.1016/j.cemconcomp.2009.08.007.
[37] K. Durst, M. Goken, M. Vehoff, Finite element study for nanoindentation measurements of two-phase materials, J. Mater. Res. 19 (1) (2004) 85–93.
[38] S.M. Ross, Introduction to Probability and Statistics for Engineers and Scientists, 4th editionAcademic Press, 2009.
[39] M. Delesse, Procédé mécanique pour déterminer la composition des roches, C. R. Acad. Sci. 25 (1847) 544–547.
[40] H. Manzano, J.S. Dolado, A. Ayuela, Elastic properties of the main species present in Portland cement pastes, Acta Mater. 57 (5) (2009) 1666–1674.
[41] K. Velez, S. Maximilien, D. Damidot, G. Fantozzi, F. Sorrentino, Determination by nanoindentation of elastic modulus and hardness of pure constituents of portland cement clinker, Cem. Concr. Res. 31 (4) (2001) 555–561.
[42] F.P. Ganneau, G. Constantinides, F.-J. Ulm, Dual-Indentation technique for the assesment of strength properties of cohesive-frictional material, Int. J. Solids Struct. 43 (2006) 1727–1745.
[43] S. Cariou, F.-J. Ulm, L. Dormieux, Hardness-packing density scaling relations for cohesive-frictional porous materials, J. Mech. Phys. Solids 56 (2008) 924–952.
[44] B. Gathier, F.-J. Ulm, Multiscale strength homogenization — application to shale nanoindentation MIT-CEE Res. Rep. R08-01, Dpt. of Civil and Environmental Engineering, Massachusetts Institute of Technology, Cambridge, MA, 2008.
[45] F.-J. Ulm, H.M. Jennings, Does C–S–H particle shape matter? A discussion of the paper 'Modelling elasticity of a hydrating cement paste' by Julien Sanahuja, Luc Dormieux and Gilles Chanvillard, CCR 37 (2007) 1427–1439 Cem. Concr. Res., 38 (8–9): 1126–1129.
[46] L. Dormieux, D. Kondo, F.-J. Ulm, Microporomechanics, J. Wiley & Sons, Chichester, UK, 2006.
[47] R.J.M. Pellenq, H. Van Damme, Why does concrete set? The nature of cohesion forces in hardened cement-based materials, MRS Bull. 29 (5) (2004) 319–323.
[48] R.J.M Pellenq, A. Kushima, R. Shahsavari, K.J. Van Vliet, M.J. Buehler, S. Yip, F.-J. Ulm, A realistic molecular model of cement hydrates, Proc. Natl. Acad. Sci. U. S. A. 106 (2009) (Early Edition 7 September 2009).
[49] A.J. Allen, J.J. Thomas, H.M. Jennings, Composition and density of nanoscale calcium–silicate–hydrate in cement, Nat. Mater. 6 (4) (2007) 311–316.
[50] J.J. Chen, L. Sorelli, M. Vandamme, F.-J. Ulm, G. Chanvillard, A coupled nanoindentation/SEM-EDX study on low water/cement ratio Portland cement paste: Evidence for C–S–H/CH nanocomposites, In Review (2009).
[51] P. Mondal, S.P. Shah, L. Marks, A reliable technique to determine the local mechanical properties at the nanoscale for cementitious materials, Cem. Concr. Res. 37 (10) (2007) 1440–1444.